



Buckling capacity of gusset plates derived from stability functions

A. Wong & V. Too

WSP Opus, Dunedin, New Zealand & JACOBS, Wellington, New Zealand.

S.Y. Vazquez Colunga & C-L. Lee

University of Canterbury, New Zealand.

ABSTRACT

Gusset Plates (GPs) when used to connect buckling restrained braces (BRBs) to beam-column joints, will be under large compression forces as BRBs are designed to sustain high axial compression loads without buckling. Therefore, it is necessary to ensure GPs do not buckle and allow BRBs to reach their expected load capacity. Current GPs design methods are based on crude assumptions such as equivalent column assumption. Therefore, they cannot accurately predict the actual GP buckling load. This study aims to find the buckling load of clipped square GPs accounting for their real geometry and variations in stiffness. Numerical finite element analyses were conducted to obtain the stiffness coefficients needed to define the GP stiffness matrix, which depends on axial force and residual stress. The buckling load of the GP can be obtained by determining the axial load that results in a singular stiffness matrix. This buckling load was compared against the Thornton and AISC design methods. The relationship between the stiffness matrix and the gusset plate connection length was also studied. The stiffness matrix obtained was also put into a GP-BRB system to calculate the buckling capacity of the system by using different connection lengths. It was found that when the connection length is over the transition line of the GP, the stiffness matrix derived on this study provides a buckling load less than the Thornton and AISC methods.

1 INTRODUCTION

1.1 Background

In frames with standard bracing, gusset plates (GPs) usually experience compression forces smaller than tension forces, because the braces they connected to are likely to buckle at a compression force smaller than the tension capacity. However, when GPs are used to connect a buckling restrained brace (BRB), which has its compression capacity typically larger than its tension capacity, they usually experience larger

compression forces and could fail prematurely due to buckling. This was proved by some experiments conducted on full-scale BRB frames, which showed that most of the GPs failed due to buckling in compression (Chou et al. 2012). Therefore, the compression strength of the GP needs to be well understood to avoid this undesired failure mode.

Current GP design methods, e.g. the Thornton method (Thornton 1984) and the AISC method (AISC 2016), calculate the GP capacity based on the assumption of an equivalent column. However, GPs are more similar to a plate than a column. This study proposes a method that accounts the effect of actual GP geometry on the buckling capacity.

In reality, most GPs have residual stresses. Therefore, this effect will be included in the proposal by using a stiffness reduction factor (*SRF*) (Lu 2011). The GP connection length (L_c) was also modified to study the relationship of how L_c affects the buckling load (P_{cr}) of GPs. The main study outcomes are to show that the use of stability functions (*SFs*) can provide a more accurate GP buckling capacity and that SFs can be implemented into a BRB system. The effect of different levels of axial loads is also studied.

The values of the stiffness coefficients in the GP stiffness matrix are directly related to the stability of GP. A loss of stability is equivalent to having a singular stiffness matrix. The corresponding axial load is the buckling load (P_{cr}). Therefore, the stiffness coefficients are also known as stability functions. In this study, the SFs of GPs will be obtained using numerical finite element methods.

1.2 Objectives

This study aims to do the following:

- Conduct a stability analysis to understand the buckling capacity of GPs.
- Study the effect of residual stresses on the SFs of GP.
- Study the variation of the SFs for different GP connection lengths.
- Compute the buckling capacity of GPs in a BRB system using their SFs.
- Compare the P_{cr} obtained from SFs against the Thornton and the AISC design methods.

1.3 Scope

This research project focuses on clipped square GPs with different connection lengths in a BRB system. A clipped square layout is a basic configuration of GP, which is symmetrical about BRB axis. One end of the analysed GP is bolted to the connection of a BRB while the other end is connected to a rigid beam-column joint (B-C joint).

2 LITERATURE REVIEW

2.1 Thornton Method

The Thornton method is commonly used to obtain the buckling capacity of a GP by using the Euler column buckling equation (Thornton 1984). It assumes the GP as an equivalent column strip and defines it based on Whitmore width b_e (Whitmore 1952) as shown in Figure 1. To consider the equivalent column, the thickness of the GP, t_g and b_e are used to calculate the cross-section area and the second moment of inertia (J). The effective length factor (Ke) depends on the boundary conditions (BCs) at both ends of the equivalent column. Thornton derived a specific length L_{ave} for GP, named as Thornton length. This length is taken from the average of three lengths L_1 , L_2 , and L_3 , which are measured from the edge of the B-C joint to the last row of the bolts, as shown in Figure 1.

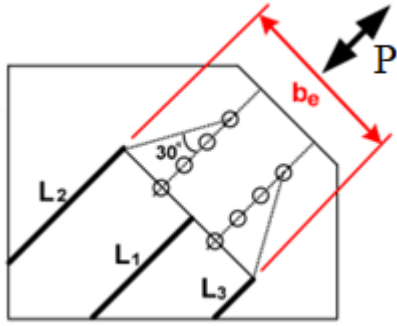


Figure 1: GP diagram indicating L_1 , L_2 , L_3 and b_e (modified from Tsai and Hsiao 2008)

Based on all these specific parameters and Young's modulus (E), the buckling capacity (P_{cr}) of GP can be computed using Equation 1. However, the limitation of the Thornton method is that the real geometry and BCs of a GP are quite different from those of a column.

$$P_{cr} = \frac{\pi^2 EI}{(KeL_{ave})^2} \quad (1)$$

2.2 AISC Method

An alternative design method is based on the AISC Specification (AISC 2016). This method is used to calculate the flexural buckling strength of members without slender elements. It can be used to obtain the buckling capacity of GPs. The P_{cr} is calculated using Equation 2, where A_g is the equivalent column cross-section area, which is defined same as the Thornton method. The F_{cr} in Equation 3 and 4 is the critical stress of the element and is depended on the element's radius of gyration (r) and effective length (KL). This method also accounts for the effects of residual stresses, out-of-plumbness and eccentric loading.

$$P_{cr} = F_{cr} A_g \quad (2)$$

$$\text{when } \frac{KL}{r} \leq 4.71 \sqrt{\frac{E}{F_y}}$$

$$F_{cr} = 0.658^{F_y/F_e} F_y \quad (3)$$

$$\text{when } \frac{KL}{r} > 4.71 \sqrt{\frac{E}{F_y}}$$

$$F_{cr} = 0.877 F_e \quad (4)$$

The elastic critical stress $F_e = \frac{\pi^2 E}{(KL/r)^2}$ and Ke are based on the BCs of the element.

3 METHODOLOGY

3.1 Obtaining stability functions

The SFs of GP are determined by representing the GP as a single element as displayed in Figure 2. It has two boundaries, End 1 and End 2, where End 1 is connected to the B-C joint and End 2 is the connection point with the BRB. The tee sections in the middle of the left diagram are the elements connecting the GP to the BRB. The SFs are found using the first principle by applying rotations (θ_i) at either end at a time and then computing their reaction moments (M_i).

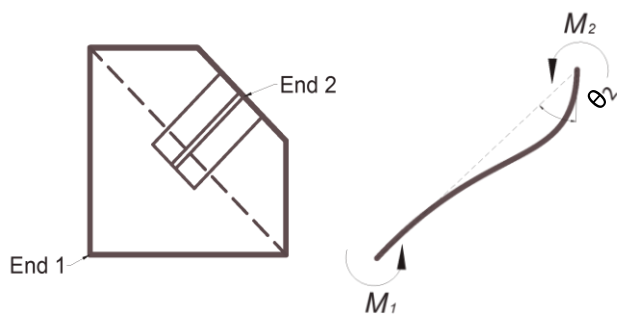


Figure 2: The concept of how GP is analysed

The relationship between M_i and θ_i of a GP are shown in Equation 5 where $A_1(P)$, $A_2(P)$, and $B(P)$ are the coefficients of the stiffness matrix of the GP (\mathbf{K}_{GP}). A_1 represents the stiffness coefficient at End 1 whereas A_2 represents the stiffness coefficient at End 2. These coefficients are the stability functions and are functions of P :

$$\begin{bmatrix} M_1 \\ M_2 \end{bmatrix} = \frac{EI}{L_{max}(1-\nu^2)} * \begin{bmatrix} A_1(P) & B(P) \\ B(P) & A_2(P) \end{bmatrix} \begin{bmatrix} \theta_1 \\ \theta_2 \end{bmatrix} \quad (5)$$

where P is the axial load, L_{max} is the maximum of L_1 , L_2 and L_3 as shown in Figure 1 and ν is the Poisson's ratio.

The method of obtaining SFs is to apply increasing levels of P to either end while keeping the rotation θ constant, this action will decrease the GP stiffness due to $P-\delta$ effect. When \mathbf{K}_{GP} becomes singular with a zero determinant ($A_1A_2 - B^2 = 0$), the corresponding load is the GP buckling load (P_{cr}) for pinned-pinned boundary conditions. This method has been validated using a beam and a rectangular plate element. The P_{cr} obtained with SFs were compared with that obtained with Euler's Column Buckling Equation and Plate Buckling Equation. To validate the accuracy of this analysis, the P_{cr} obtained with the SFs was also compared with that obtained with a buckling analysis available in the finite element analysis software ABAQUS (Simulia 2014). In addition, it was verified that the coefficient B remains the same when force is applied at either end, because of the symmetry property of a stiffness matrix.

The effect of residual stress was included through a stiffness reduction factor SRF defined in Equation 6 which was used to modify the material Young's modulus E (Lu 2011),

$$SRF = 1 - \frac{\frac{N^*}{b e^* t_g^* F_y}}{1 + c \left(1 - \frac{N^*}{b e^* t_g^* F_y} \right)} \quad (6)$$

where $c = 1.5 * e^{-1.8\alpha_b} - 0.35$, N^* is the axial load applied to the GP, α_b is defined as 0.5 for a flame cut plate (Standards New Zealand 1997). The P_{cr} obtained from this method was then compared to the Thornton and the AISC method.

3.2 Changing GP connection length

After obtaining the SFs of the GP, the connection length L_c of the GP, as shown in Figure 3, was modified. The dashed line in the figure represents the bending line that connects the GP top left corner to the GP bottom right corner. The length L_c was modified 4 times from a length including 3 to 6 rows of bolts while everything else remained unchanged. These lengths were selected because they vary around the bending line and therefore they show how the SFs change close to the bending line. A model was created for each modification to compute the coefficients and ten incremental loads were applied to provide a better curve of the coefficients.

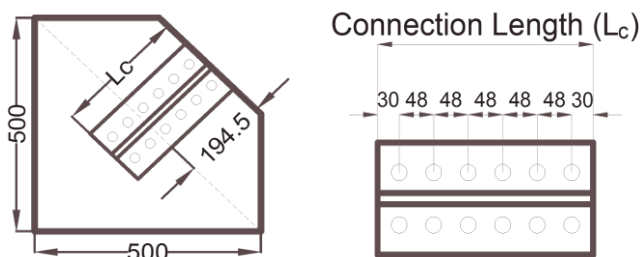


Figure 3: GP variable connection length

3.3 GP-BRB system buckling load

The buckling load of a GP-BRB system was computed by obtaining the axial load that results in a singular system stiffness matrix. The system stiffness matrix was assembled using the direct stiffness method. Figure 4 shows the layout of the GP-BRB system with fixed BCs at both ends. The system has eight degrees of freedom (DOFs) which are 4 translational and 4 rotational. The $P-\Delta$ effect on the rigid body modes of each element caused by a rotation of element chord can be incorporated by introducing the geometric stiffness $K_{P\Delta}$, shown in Equation 7, for each element of length L_e :

$$K_{P\Delta} = \frac{-P}{L_e} \begin{bmatrix} 1 & -1 \\ -1 & 1 \end{bmatrix} \quad (7)$$

The BCs of the system depend on the GP's end that connects to the B-C joint. This research focused on fixed-fixed and pinned-pinned BCs. To obtain the system stiffness matrix, the SFs of each element on the system are needed. The SFs of GPs from previous sections were used while the SFs for the connection and BRB are assumed to be the same as a normal beam element.

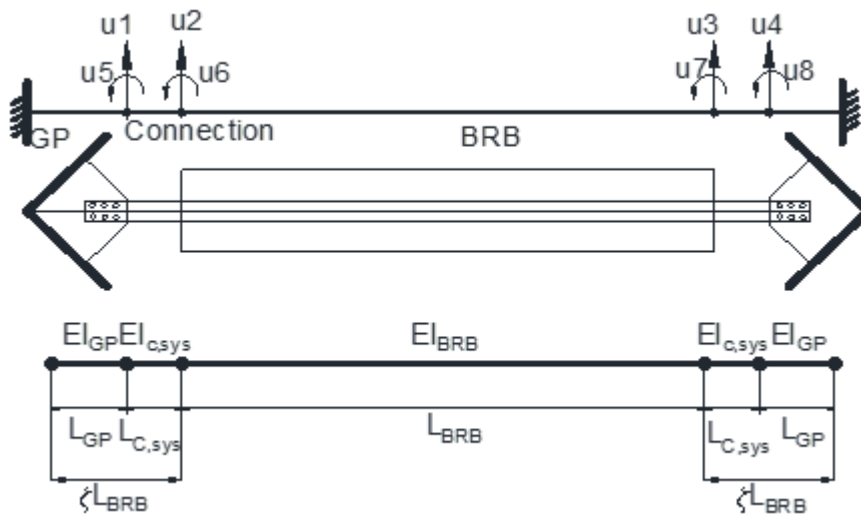


Figure 4: Layout of the GP-BRB system

The exact solution for A and B of a typical beam element are shown in Equation 8a and 8b:

$$A_1 = A_2 = \frac{\psi(\sin(\psi) - \psi \cos(\psi))}{2 - 2 \cos(\psi) - \psi(\sin(\psi))} \quad (8a)$$

$$B = \frac{\psi(\psi - \sin(\psi))}{2 - 2 \cos(\psi) - \psi(\sin(\psi))} \quad (8b)$$

where $\psi = \sqrt{P \times \frac{L^2}{EI}}$, and P is the axial force in the system. Using the same approach for obtaining the P_{cr} for a GP, the buckling load of the system can be found.

4 MODELS

4.1 Model of GP

The analysis was performed numerically using finite element software ABAQUS. Figure 5a and 5b shows the numerical model and the geometry of the square GP analysed, respectively. All numbers are in mm.

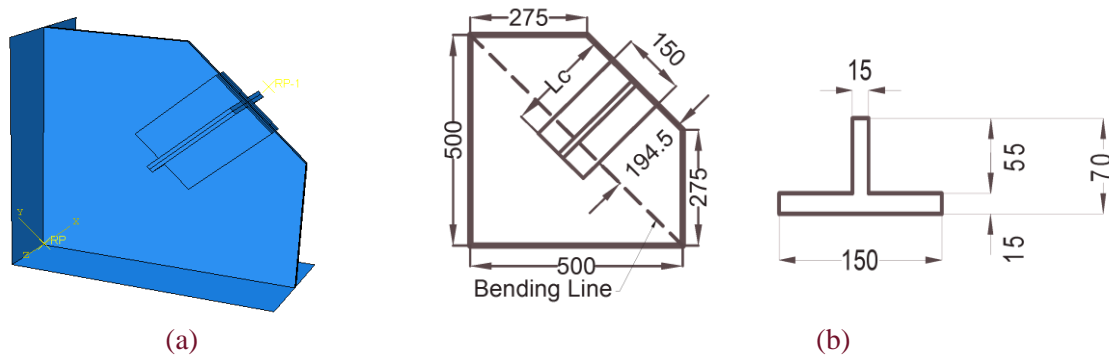


Figure 5: a) Finite element model and b) GP and connection geometry

Each GP was modelled as an element with pinned-pinned BCs. Three types of elements were defined: rigid joint, tee sections, and GP. The joint was assumed rigid as it is connected to the B-C joint. It was defined as a 3D discrete rigid element in ABAQUS while all other elements were defined as deformable shell elements. For the GP and tee sections, E was defined as 210 GPa and had an inelastic material property of yield strength $F_y = 300$ MPa. The GP had a thickness of 8 mm while the tee sections was 15 mm. A mesh size of 15 mm was used for all elements and tie constraints were used to connect the rigid joint and tee sections to GP. The bolts were assumed to be rigid using rigid beam elements. The bolts were coupled at all the DOFs that were in contact from the tee sections and GP plate at the location of the bolts. Between the connection and plate surfaces, hard contact was prescribed. When varying the connection length L_c , only L_c changed with increasing rows of bolts while all other parameters remained the same.

4.2 Model of GP-BRB system

A realistic configuration of a GP-BRB system was found based on some research on existing experimental data (Takeuchi et al. 2013). Figure 4 shows the layout of the lengths allocated. The length of BRB (L_{BRB}) was assumed to be quadruple the sum of the lengths of connection in system ($L_{c,sys}$) and length of the GP (L_{GP}). At the same time, the EI_{BRB} was double the $EI_{c,sys}$, and they were based on the EI factor of the GP. I_{GP} was based on the b_e and t_g as the width and height respectively, while $E = 210$ GPa. Therefore, the length of the L_{GP} used was 548 mm, $L_{c,sys}$ 400 mm and L_{BRB} 3800 mm.

5 RESULTS AND DISCUSSIONS

5.1 Stiffness coefficients

Using finite element models built in ABAQUS and the previously described methodology, the numerical analyses gave the reaction moments on different ends of the GP. Therefore, the stability functions A_1 , A_2 , and B , of a typical GP with L_c of 156 mm were found and shown in Figure 6a. The coefficients have been normalised by $EI/L_{max}(1 - \nu^2)$. They are plotted against the P normalised by $Pe = \pi^2 EI/L_{max}^2$. The buckling load of the GP with the pinned-pinned BCs was found when $A_1 A_2 - B^2 = 0$, marked with a red circle in Figure 6b. As shown in the figures, the increment of load P was not uniform so when putting the SFs of GP into GP-BRB system, linear interpolation was done between each data point to get the value of the coefficient. Unlike a typical beam where both A_1 and A_2 will have the same value of 4 at $P = 0$, the coefficients are around 10 times larger than that of a beam. The value of A_2 is bigger than A_1 while B value is decreasing. The reason could be due to the way b_e and BCs are specified. The b_e used in the modelling is the Whitmore width, but it is believed that if b_e accounts for an elliptical width around the connection, it should be bigger. This will result in a bigger value of I and the factor that normalises the coefficients, so the values of stiffness coefficients will be lower.

Nevertheless, this result still contradicted with what was expected. It was expected that when L_c passed bending line, A_2 would be bigger than A_1 as more stiffness in B-C joint (A_1) would contribute to the connection joint stiffness (A_2). But this is not the case for L_c of 156 mm so further investigation is required to determine the likely reason.

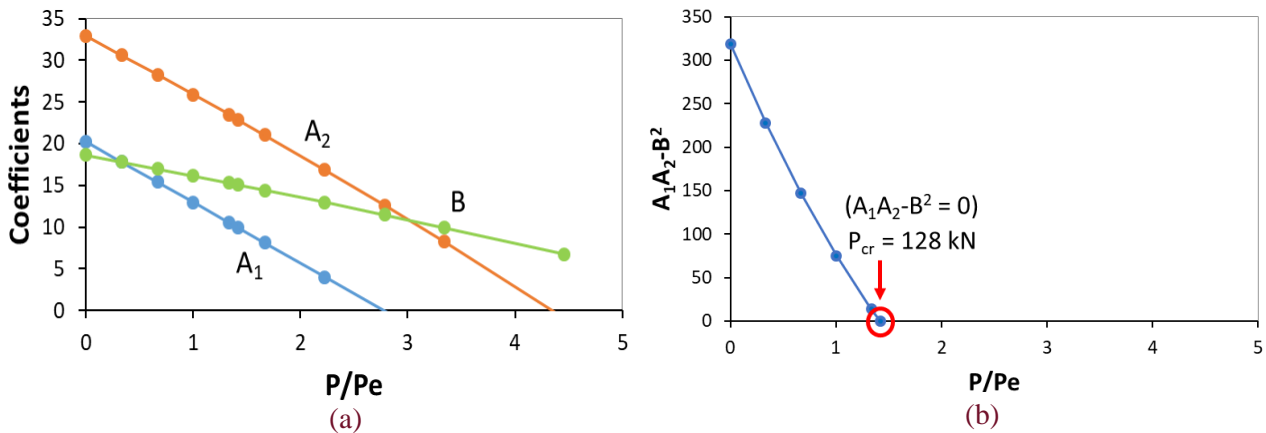


Figure 6: a) GP stability functions and b) Variation of $A_1A_2 - B^2$

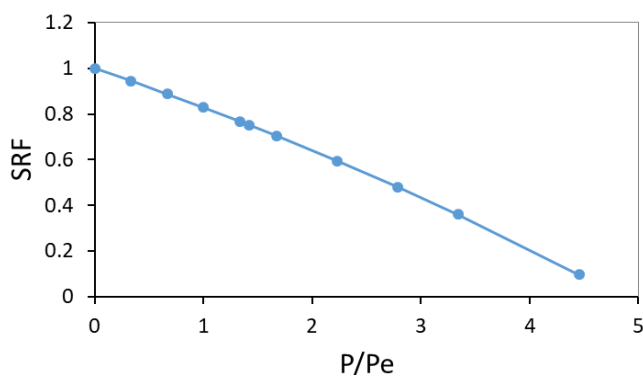


Figure 7 shows the variation of SRF versus P/Pe . It can be seen that as the axial force increased, SRF decreased. Thus, a greater load will have a greater residual stresses effect on the GP. The P_{cr} with SRF was obtained by multiplying the factor with the P_{cr} . For a GP with L_c of 156 mm, P_{cr} was 128 kN without SRF and 96 kN with SRF.

Figure 7: Variation of SRF with axial load

5.2 The modification of GP L_c

The L_c was modified four times for connection ranging from 3 to 6 rows of bolts. Figure 8 shows the result of how the A_1 and A_2 coefficients changed with different L_c . The data was labelled by their respective L_c values.

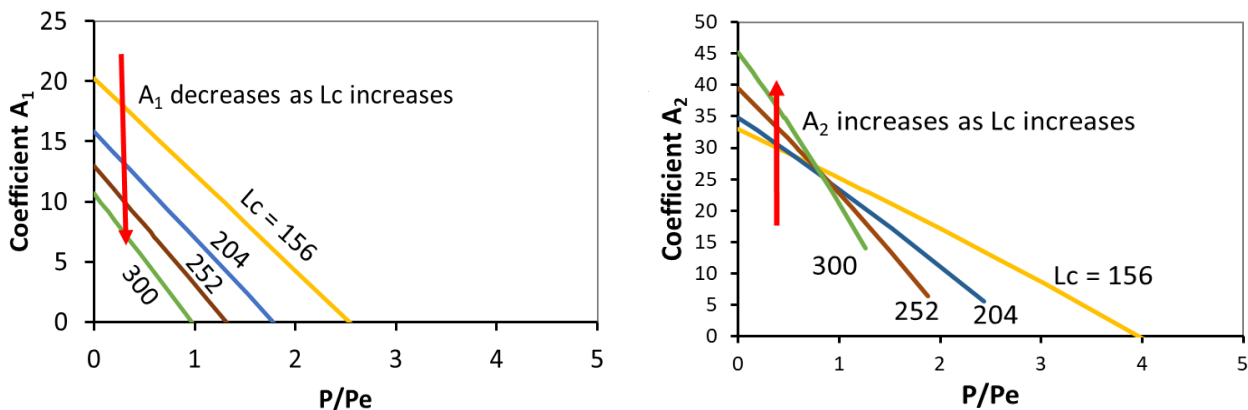


Figure 8: Variation of stiffness coefficients A_1 and A_2 with L_c

The results show that as L_c increases, A_1 decreases and A_2 increases. This is expected because when the connection gets longer, the maximum distance between the connection and B-C joint, L_{max} , decreases. When it deforms due to the load applied, the stiffness at the corners of the B-C joint (A_1) will contribute to the connection joint stiffness (A_2). It can also be seen that for A_2 , the slopes become steeper as L_c increases. This is caused by the P/Pe factor. The factor is proportional to L_{max}^2 which get smaller as L_c increases.

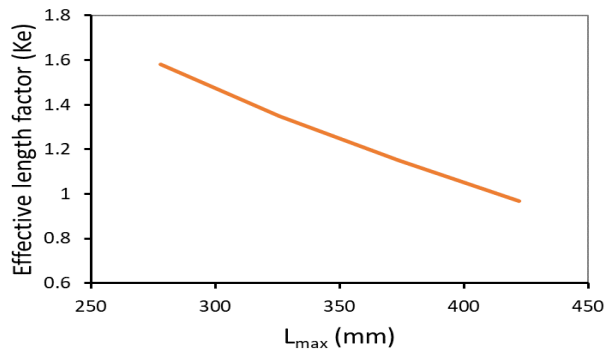


Figure 9: Variation of Ke with L_{max} for P_{cr} of GP without SRF

increases with increasing L_c , as expected. The buckling load including SRF has lower values because residual stresses lower the GP capacity. The gap between P_{cr} with and without SRF also becomes bigger as L_c increased. This can be explained by Equation 6 where SRF and N^* has an inversely proportional relationship. Hence, as P_{cr} increases more, SRF decreases more.

Figure 9 shows the variation of the Ke needed to obtain the P_{cr} obtained as L_{max} changes. The value of effective length factor Ke is found by taking the square root of P_{cr} over Pe . As shown in the graph, Ke becomes bigger when L_{max} decreases. This is expected because Ke gets smaller when element is more restrained.

In addition, Table 1 shows how P_{cr} with and without SRF changes with different L_c . Regardless of the effect of SRF , it can be seen that P_{cr}

Table 1: Buckling load of GPs with and without SRF

L_c (mm)	P_{cr} without SRF (kN)	P_{cr} with SRF (kN)
156	128	96
204	143	113
252	167	134
300	199	159

5.3 GP-BRB system

In a typical GP-BRB system, the GP should be stronger than the BRB, so the buckling load of the system will not be dependent on the GP buckling capacity itself. Therefore, using the same approach in obtaining the P_{cr} of GP, the system P_{cr} ($P_{cr, s}$) is obtained by substituting the SFs of GPs into the BRB system. According to the system's properties and configuration mentioned, Table 2 shows the $P_{cr, s}$ of the BRB system with fixed-fixed and pinned-pinned BCs.

Table 2: $P_{cr, s}$ of BRB system.

L_c (mm)	$P_{cr, s}$ (kN)	
	Fixed-fixed	Pinned-pinned
156	110	35
204	176	38
252	274	40
300	436	42

As seen from Table 2, when the L_c of GP increases, the system capacity increases. However, the $P_{cr,s}$ with pinned-pinned BCs was less than half of the $P_{cr,s}$ in the fixed-fixed BCs. The reason for this difference is due to the effective length of GP. Fixed-fixed BCs provide more restraints to the elements, resulting in a smaller effective length and a higher capacity of the system.

When comparing P_{cr} of GP to $P_{cr,s}$, it is expected that $P_{cr,s}$ will be smaller. This is because one end of the GP in a GP-BRB system is allowed to move laterally, resulting in a less stable system than GP alone. Hence, in design, a more realistic buckling capacity of the GP will be provided by $P_{cr,s}$ instead of the P_{cr} of the GP as the BCs of the GP can be better represented for a GP-BRB system.

However, the $P_{cr,s}$ results in Table 2 are different from what is predicted. The $P_{cr,s}$ from fixed-fixed BCs is too big while in pinned-pinned BCs is too small when compared to P_{cr} of GP. The reason is possibly due to the assumptions made for EI_{BRB} and $EI_{c,sys}$, which are based on a ratio of EI_{GP} . If they are based on physical dimensions rather than ratio then the result is likely to be more appropriate. Nevertheless, the $P_{cr,s}$ obtained from fixed-fixed BC is still more realistic so in the following section, the comparison will focus on the GP-BRB system with fixed-fixed BCs.

5.4 Comparison with other methods

The P_{cr} of the GP obtained from SFs, Thornton and AISC methods for different L_c are shown in Figure 10. The P_{cr} of Thornton and AISC methods were obtained using $Ke = 1.2$ and 2 , where 1.2 is proposed by the AISC method. As AISC considers the effect of residual stress and initial imperfections, its P_{cr} is expected to be lower than the P_{cr} from the Thornton method. The SFs are also predicted to provide a bigger P_{cr} than the other design methods, since the design methods are expected to be conservative.

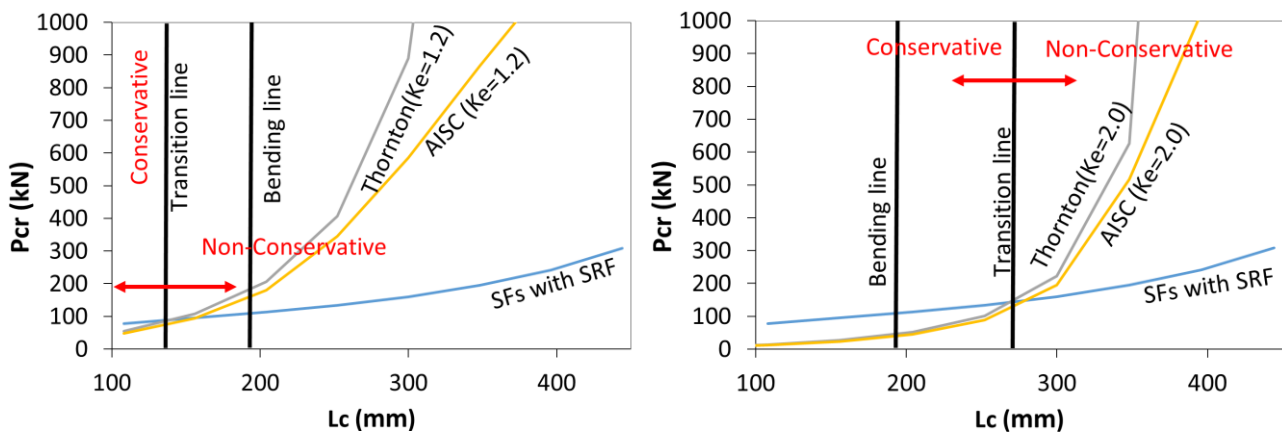


Figure 10: The P_{cr} from SFs, Thornton and AISC methods for $Ke = 1.2$ and 2

The transition line in Figure 10 represents the value of L_c when the design methods provide a similar P_{cr} to the SFs (with SRF). When the design methods produce a lower value of P_{cr} than SFs, they are said to be conservative for design. According to Figure 10, before the transition line, the results of the design methods lies in a conservative zone. Conversely, for L_c greater than the value of the transition line, the design methods provide non-conservative estimate of P_{cr} .

As shown, the transition line for $Ke = 2$ occurs later than $Ke = 1.2$ so the design methods provide a more conservative result when $Ke = 2$ rather than $Ke = 1.2$. However, both Ke factors will provide non-conservative designs when the L_c increases to more than 5 rows of bolts. Most of the GP-BRB design will have a configuration of L_c greater so these two design methods will not give a conservative estimate of P_{cr} .

As the AISC method provided a more conservative result, the following investigation would compare SFs with the AISC method. The $P_{cr,s}$ was compared with the AISC method for different L_c and Ke values.

Figure 11 shows the $P_{cr, s}$ in dashed lines and P_{cr} from AISC method in solid lines. The red dots represent the required Ke values for different L_c in AISC method to obtain the same $P_{cr, s}$.

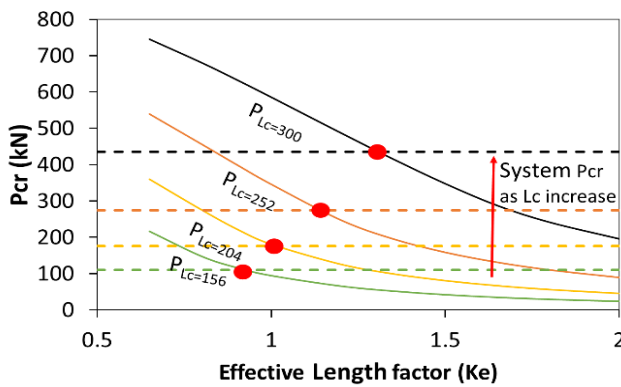


Figure 11: Variation of system and AISC P_{cr} with effective length factor

As $P_{cr, s}$ is a more realistic result for the P_{cr} of the GP, the value of AISC P_{cr} should be smaller than $P_{cr, s}$ for a conservative design. According to Figure 11, when $Ke = 2$, all the AISC P_{cr} in various L_c provided lower values than $P_{cr, s}$. Unlike the result from Figure 10, the results of $P_{cr, s}$ show that when L_c and Ke increase, conservative estimates of P_{cr} can be found using AISC method. Since L_c and L_{max} has an inverse relationship and L_{max} represents the buckling length that was used in the Thornton and AISC methods, the increase in L_c will cause L_{max} to decrease. As L_{max} decreases, the Ke value has to increase to maintain the same P_{cr} of

the GP. Therefore, to obtain a realistic P_{cr} in the Thornton and the AISC methods, a larger Ke will be required.

Table 3 also shows the ratio of P_{cr} from AISC method (P_{AISC}) with $Ke = 1.2$ and 2 over $P_{cr, s}$ with different L_c . This shows the conservative level of the AISC design method.

From the table, the AISC method when $Ke = 2$ provided a too conservative P_{cr} to the GP as they are less than half of the $P_{cr, s}$. On the other hand, one of the results has exceeded 1 when $Ke = 1.2$ suggesting they are non-conservative. Hence, it is proposed that the Ke value should be different for different L_c of GP to provide a result within a reasonable range of conservativeness level.

Table 3: Ratio of P_{AISC} to $P_{cr, s}$ with different L_c .

L_c (mm)	$P_{AISC}/P_{cr, s}$ (kN)	
	$Ke = 1.2$	$Ke = 2.0$
156	0.6	0.25
204	0.7	0.26
252	0.9	0.32
300	1.1	0.45

6 CONCLUSIONS AND RECOMMENDATIONS

The stability analysis was used to determine the buckling capacity (P_{cr}) of the GP with different connection lengths (L_c) and compared with the BRB system. The following conclusions were drawn from the results:

1. GPs have different stability functions (SFs) from beams.
2. An increase in L_c causes an increase in stiffness at its connection end, as the stiffness from the beam-column joint provides contributions.
3. The inclusion of the effect of residual stresses will decrease the P_{cr} of GP.
4. As L_c increases, the P_{cr} of the GP also increases because of the stronger stiffness provided by a longer connection.

5. In a GP-BRB system, the $P_{cr, s}$ provided more realistic results than the P_{cr} of the GP due to a better representation of boundary conditions on the GPs.
6. When using the design methods, a bigger value of Ke will be required for computing a conservative and accurate estimation of the GP capacity. However, according to P_{cr} from SFs, design methods become more non-conservative when L_c increases passing the transition line.
7. On the other hand, compared to $P_{cr, s}$, the P_{cr} from the AISC method provides similar results to SFs by using $1.2 < Ke < 2.0$, which depends on L_c . This Ke value should not be a fixed value as proposed in the AISC method.
8. The SFs represents an alternative method to obtain the buckling capacity of a GP on a BRB system. However, further study is necessary to account for a wider range of GP and BRB configurations. Realistic BRB-GP configurations and boundary conditions are also needed in order to provide a more accurate estimation of the GP stability functions and buckling load.

7 REFERENCES

- American Institute of Steel Construction (AISC). 2016. *Specification for structural steel buildings*, American Institute of Steel Construction (AISC), 360–16, Chicago.
- Chou, C.C., Liu, J.H. & Pham, D.H. 2012. Steel buckling-restrained braced frames with single and dual corner gusset connections: seismic tests and analyses, *Earthquake Engineering & Structural Dynamics*, Vol 41(7) 1137-1156.
- Lu, A. 2011. *Effects of member overstrength and initial residual stresses on the behaviour of 2D steel structure*, University of Canterbury, Christchurch.
- Simulia. 2014. *ABAQUS analysis user's manual*. Version 6.14; 2014.
- Standards New Zealand. 1997. *Steel Structures standard NZS3404*, Standards New Zealand, Wellington.
- Takeuchi, T., Ozaki, H., Matsui, R. et al. 2013. Out-of-plane Stability of Buckling-Restrained Braces Including Moment Transfer Capacity, *Earthquake Engineering & Structural Dynamics*, Vol 43 851-869.
- Thornton, W.A. 1984. Bracing connections for heavy construction, *Engineering Journal*, Vol 21(3) 139-148.
- Tsai, K.C. & Hsiao, P.C. 2008. Pseudo-dynamic test of a full-scale CFT/BRB frame—Part II: Seismic performance of buckling-restrained braces and connections, *Earthquake Engineering & Structural Dynamics*, Vol 37(7) 1099-1115.
- Whitmore, R. 1952. *Experimental investigation of stresses in gusset plates*, Engineering Experiment Station, University of Tennessee.